CHALMERS UNIVERSITY OF TECHNOLOGY
Gothenburg, Sweden
www.chalmers.se

LICENTIATE THESIS

KESAVAN SEKAR • Multiscale characterization of hierarchical nanostructured fluid flows • 2025

Multiscale characterization of hierarchical nanostructured fluid flows

KESAVAN SEKAR

DEPARTMENT OF INDUSTRIAL AND MATERIALS SCIENCE
CHALMERS UNIVERSITY OF TECHNOLOGY
Gothenburg, Sweden 2025
www.chalmers.se

THESIS FOR THE DEGREE OF LICENTIATE OF ENGINEERING

Multiscale characterization of hierarchical nanostructured fluid flows

Kesavan Sekar

Department of Industrial and Materials Science
Chalmers University of Technology
Gothenburg, Sweden, 2025.

Multiscale characterization of hierarchical nanostructured fluid flows

KESAVAN SEKAR

Technical Report No.IMS-2025-09
This thesis has been prepared using LaTeX.

Department of Industrial and Materials Science
Chalmers University of Technology
SE-412 96 Gothenburg, Sweden
Phone: +46 (0)31 772 1000
www.chalmers.se

Printed by Chalmers Reproservice
Gothenburg, Sweden, May 2025

Abstract

Natural hierarchical materials such as wood and bone exhibit multifunctional properties due to their precise orientation and alignment across multiple length and time scales. The study of material'building blocks' capable of forming such hierarchies, usually from the point of view of 'self-assembly' is inspired by such natural materials. Among the many examples, one-dimensional (1D) rod-like cellulose nanocrystals (CNCs) and two-dimensional (2D) Graphene oxide (GO) platelets can self-assemble in water into hierarchical structures spanning from atomic, molecular, primary nanoparticles, mesoscale structures thereof to macroscale structures. These mesoscopic domains can take the form of liquid crystalline phases (E.g., nematic, chiral nematic etc. phases), which govern their positional and directional ordering. Such ordering can be utilized to achieve high throughput. However, the inherent structural complexity across scales necessitates simultaneous multiscale characterization to understand and control their behavior during processing. This PhD project focuses on developing and applying advanced hyphenated rheological techniques, i.e. combining rheology with microscopy and scattering to elucidate how these materials reorganize under deformation and flow. A novel integration of rheology, polarized light imaging (PLI), and small-angle X-ray scattering (SAXS) enabled real-time observation of orientation propagation under simple shear. Furthermore, a Taylor–Couette (TC) geometry, combined with SAXS, revealed the interplay between particle morphology and/or size and vortex structures during transitional flow. To explore the evolution of mesoscopic structures, we are also developing a new technique that couples rheology with nonlinear optics. Overall, this research establishes comprehensive techniques for probing structure-property relationships across length and time scales, and lays the groundwork for hierarchical control in processing applications such as 3D printing.

Keywords: Hierarchical systems, cellulose nanocrystals (CNCs), Graphene oxide (GO), advanced rheological techniques, polarized light imaging (PLI), small-angle X-ray scattering (SAXS), Taylor-Couette (TC) instabilities, nonlinear optics

List of Publications

This thesis is based on the following publications:

[**A**] Reza Ghanbari, Ann Terry, Sylwia Wojno, Marko Bek, **Kesavan Sekar**, Amit Kumar Sonker, Kim Nygård, Viney Ghai, Simona Bianco, Marianne Liebi, Aleksander Matic, Gunnar Westman, Tiina Nypelö, Roland Kádár. "Propagation of Orientation Across Lengthscales in Sheared Self-Assembling Hierarchical Suspensions via Rheo-PLI-SAXS" *Advanced Science*, 12(7), 2410920.

[**B**] [**Kesavan Sekar**], Viney Ghai, Reza Ghanbari, Kim Nygård, Ann Terry, Roland Kádár. "Influence of nanoparticle morphologies in Taylor-Couette flow transitions". Manuscript.

[**C**] [**Kesavan Sekar**], Viney Ghai, Reza Ghanbari, Marko Bek, Marianne Liebi, Aleksander Matic, Ann Terry, Kim Nygård, Roland Kádár. "Multi-scale transitional flow in anisotropic nanoparticle suspensions". Manuscript.

Publications not included in this thesis, are:

[**A**] Reza Ghanbari, Sajjad Pashazadeh, **Kesavan Sekar**, Kim Nygård, Ann Terry, Marianne Liebi, Aleksander Matic, Roland Kádár. "Painting Taylor vortices with cellulose nanocrystals: Suspension flow supercritical spectral dynamics." *Physics of Fluids*, 36.4 (2024).

Acknowledgments

I would like to express my sincere gratitude to my supervisor and mentor, Prof. Roland Kádár, for his invaluable support and guidance. Thank you for trusting me and encouragement to explore this field further.

I would also like to thank my co-supervisors, Dr.Kim Nygård and Dr.Ann Terry from MAX IV, for their support and technical insights.

I would like to extend my gratitude to all the group members for their input, help during the experiments and all the afterwork in the Rheology and Processing of Soft Matter Laboratory.

Finally, I would like to thank my family and friends for their unwavering support, encouragement and love.

This work has been conducted within the Wallenberg Wood Science Center (WWSC) and I gratefully acknowledge their financial support.

Acronyms

CNC:	Cellulose nanocrystal
GO:	Graphene oxide
SAXS:	Small-angle X-ray scattering
PLI:	Polarized light imaging
POM:	Polarized optical microscopy
TEM:	Transmission electron microscopy
TC:	Taylor-Couette
1D:	One-dimension
2D:	Two-dimension
LCF:	Laminar Couette Flow
PTVF:	Pre Taylor Vortex Flow
TVF:	Taylor Vortex Flow
WVF:	Wavy Vortex Flow
MWV:	Modulated Wavy Vortices
CWV:	Chaotic Wavy Vortices
C/MWV:	Chaotic Modulated Wavy Vortices
WTV:	Wavy Turbulent Vortices
TWV:	Turbulent Wavy Vortices
TTV:	Turbulent Taylor Vortices
TI:	Turbulent Instabilities
S:	Spirals

IS:	Interpenetrating Spirals
WS:	Wavy Spirals
CS/W:	Chaotic Spiral Waves
2D-FFT:	Two dimensional fast Fourier Transform
Re:	Reynolds number
Wi:	Weissenberg number
El:	Elasticity number
NLO:	Non-linear optics
SHG:	Second harmonic generation
TPEF:	Two-photon excited fluorescence
P:	Polarizer
A:	Analyzer
QWP:	Quarter waveplate
BS:	Beamsplitter
M:	Mirror
L:	Objective lens
TL:	Tube lens
D:	Detector
PP:	Parallel plate
DG:	Double gap

Contents

Part I

Overview

CHAPTER 1

Introduction

1.1 Hierarchical systems

Hierarchical systems comprise various ordered and dissordered domains across length scales ranging from Ångstrom to meter length scales. A prime example of such is wood. Wood primarily consists of three biopolymers: cellulose, hemicellulose and lignin. Hierarchy originates from cellulose molecular chains to elementary fibrils to microfibril bundles, which contain amorphous and crystalline regions embedded in a lignin and hemicellulose matrix within the cell walls, which then organize into macroscale structures. This unprecedented level of cellulose orientation across multiple length scales significantly contributes to the excellent mechanical properties [1]. One strategy to mimic natural hierarchical systems, and thus avoid the long time scales associated with e.g. the growth of a tree, is by using primary building blocks - whether naturally occurring or not - that possess the potential for building up hierarchies. Such building blocks include cellulose nanocrystals (CNCs), which are one-dimensional (1D) rod-like nanoparticles, and Graphene oxide (GO), which are two-dimensional platelets. These materials, when dispersed in water, can self-assemble into hierarchical liquid crystalline phases such as nematic and chiral nematic phases [2], [3]. Apart from these phases, multiple structures coexist depending on sample preparation and surface charges, leading to agglomerates and aggregates in a suspension[4]. This creates an unprecedented level of complexity while characterizing such systems by rheology. Rheology helps us understand how materials flow and deform in response to stress and shear[5]. However, rheology outputs the average or bulk measure of the material characteristics. The coupling of different characterization techniques with rheology is necessary to localize the multiscale mechanisms of the material response, in order to control their assembly into formed materials and the ensuing material properties [6]–[8].

1.2 Multiscale dynamics

Suspension dynamics include multiple structures (Nematic, chiral nematic, agglomerates, aggregates) across different length scales, that must be understood to tailor the final product properties. Achieving hierarchical orientation using hydrodynamic flow fields is essential to increase throughput. How does the hydrodynamic flow field interact with matter and restructure the different phases inside the suspension? This can be understood through various rheological and flow stability tests such as Taylor-Couette (TC) flow i.e flow between rotating cylinders. TC experiments have been widely used to study the onset and development of instabilities and the factors that influence flow stability [9], such as the interplay between inertia, elasticity, particle morphologies, flow domain parameters, etc. In the TC flow for a Newtonian fluid, the transition starts with Laminar Couette flow (LCF). where the fluid follows a circular trajectory. Then, with an increase in Re, the flow destabilizes towards its primary instability where Taylor vortices start to appear as Taylor vortex flow (TVF) identified upon its one spatial frequency. Later, upon further increase in Re, secondary flows appear as Wavy vortex flow (WVF) with one temporal and spatial frequency, modulated wavy vortices (MWV) with two spatial and one temporal frequency, Chaotic wavy vortices (CWV) with a background noise present in the space-time diagrams originating from the merging and splitting of vortices[10]–[16]. Hydrodynamic shear impacts the structuring during its transition from laminar to turbulent through secondary flow transitions originating from the propagation of vortices across multiple length scales and its relation to stabilize or destabilization of the flow leading to various inertial, elastic instabilities can be seen in Taylor-Couette flow stability experiments [17]. The above methods provide a macroscopic or flow scale understanding of the suspension.

In addition, non-linear optical microscopy (NLO), especially second-harmonic generation (SHG) microscopy, offers several advantages over conventional optical microscopy techniques. Owing to its coherent, structure-specific interaction with materials and the use of near-infrared excitation, SHG microscopy provides reduced scattering and deeper penetration in biological and soft matter systems[18]. Recent experiments have shown that cellulose nanocrystals (CNCs), due to their noncentrosymmetric crystal structure, generate detectable SHG signals, enabling label-free visualization and orientation mapping[19]. Furthermore, by incorporating appropriate spectral filters, it is possible to simultaneously image two-photon excited fluorescence (TPEF) alongside SHG, allowing for multimodal contrast in a single imaging system. By combining rheology with different techniques such as scattering, microscopy, and spectroscopy, material response originating from molecular to micro to meso to macroscopic level can be better understood simultaneously rather than being complemented later through separate experiments.

Hyphenated techniques include rheology coupled to small-angle scattering (Rheo-SAXS)and wide-angle scattering (Rheo-WAXS) for nano-macro understanding as well as polarized light imaging (Rheo-PLI) for meso-macro understanding of the dynamics[6], [8], [20], [21]. In this thesis, we focus on three new techniques we have developed and are working to achieve a multi-scale understanding of fluid flows. Here, a new double-hyphenated technique (Rheo-PLI-SAXS), Taylor-Couette flow coupled to SAXS (TC-SAXS) and a new nonlinear optics coupled to rheology (Rheo-NLO) will be discussed.

1.3 Motivation and research question

Multiple lengths and time scales contribute to the structuring or restructuring of the material, resulting in various properties. Multiple techniques combined with rheology are needed to further expand our understanding of these hierarchical systems. However, the material complexity and characterization methods without coupling limit our proper understanding of these systems simultaneously. This PhD project aims to develop relevant hyphenated techniques coupled with rheology to understand better how flow-induced structuring happens during processing.

For that, we are exploring

- A new double hyphenated technique (Rheo-PLI-SAXS) taking advantage of rheology, scattering and polarized light imaging [nano-micro-macro] - Paper I
- Influence of 1D and 2D nanoparticles in TC flows - Paper II
- Coupling Taylor-Couette flow to SAXS and polarized light imaging to probe the destructuring of the hierarchical systems in transitional flows [nano-macro] - Paper III
- New nonlinear optical train coupled to rheology to have more local understanding up to nanosecond timescales [meso-macro]

CHAPTER 2

Materials and methods

2.1 Materials

Multiple hierarchical systems have been explored, mainly cellulose nanocrystals (CNC) and Graphene oxide (GO). These particles can self-assemble into hierarchical structures when dispersed in water and also vary based on concentration, surface charges, dimensions, etc. Here, the 1D CNCs can self-assemble into chiral nematic liquid crystalline domains, whereas 2D GO can self-assemble into nematic liquid crystalline phases. In addition to the above, surface-modified [P]-CNC-OH-2-Prop-C_2-N-C_2 CNCs and rigid thin wall nanotube suspension have also been studied in Paper-I. Hybrid systems of CNC and GO have also been explored in Paper-II.

Rheology

Rheological properties of all the suspensions has been carried out in Anton Paar 702 Multidrive rheometer in single and twin drive transducer configuration. Mainly two types of geometries were used: a) glass parallel-plate with 43mm diameter, b) double gap geometry with inner bob 27 mm diameter.

Steady shear measurements were done using custom procedure where transient data measured at each point for a certain amount of time. Shear rate was varied between 0.001 and 100 s^{-1} In the case of CNCs, based on sample preparation protocol, rheological characteristics varied where probe sonication reduced the amount of agglomerates present in the sample leading to reduced viscosities and shear thinning nature depending upon concentration. Three region viscosity curves were seen: i) due to the presence of agglomerates with mesoscopic domains in region-I, ii) breakup of those structures revealing shear thinning region, iii) the above structures further broken down into flow aligned domains/clusters of nanoparticles. GOs exhibited a shear-thinning behaviour in steady shear measurements. Moreover, GO had a crossover seen in terminal region of the dynamic frequency sweep tests between 0.001 and 100 rad/s^{-1} at constant strain amplitude of 1%.

Taylor-Couette flow

A custom Taylor-Couette (TC) geometry with independently rotating cylinders, mounted on an Anton Paar 702e Space rheometer, has been used for the flow stability experiments. An inner polycarbonate cylinder with a 41 mm diameter and an outer glass cylinder with a 45 mm diameter were used to allow the transmission of polarized light. Two linear polarizers were oriented at 90^0 relative to each other to create a cross-polarized setup, allowing for the visualization of instabilities through the inherent birefringence of the nanoparticle suspensions without the need for additional visualization aids, which affects the material's microstructure. The Canon 90D DSLR camera captured the instabilities at a 100 fps frame rate in Full HD format (1920x1080 px). From these videos, 1 pixel from each frame along the rotation axis of the cylinders was extracted and stacked to form a space-time plot. Furthermore, a 2D Fourier Transform (2D-FFT) was performed on these space-time plots to identify the onset of the instabilities by obtaining the characteristic temporal frequency, f, and spatial wavenumber, κ.

Reynolds number is used to account for the ratio of inertial and viscous forces,

$$Re_{(i,o)} = \frac{\rho \cdot R_{i,o} \cdot |\Omega_{i,o}| \cdot d_\beta}{\eta(\dot{\gamma})} \tag{2.1}$$

- i,o - inner and outer cylinder

- ρ - density of the suspensions
- $|\Omega| = \Omega_i + |\Omega_o|$ - Total angular velocity
- $\eta(\dot{\gamma})$ - Shear-rate dependant viscosity
- d_β denotes relative gap between two cylinders

$$d_\beta = \begin{cases} d \cdot (1 - |\beta|) & \text{if } Re^{(i,o)} = Re^{(i)}, \\ d \cdot |\beta| & \text{if } Re^{(i,o)} = Re^{(o)}, \end{cases} \tag{2.2}$$

where

$$\beta = \frac{\Omega_o}{\Omega_i + |\Omega_o|} \tag{2.3}$$

- $\beta = 0$ - Inner cylinder (rotating) and outer cylinder (rest)
- $\beta = -1$ - Outer cylinder (rotating) and inner cylinder (rest)
- $\beta = -0.25, -0.5, -0.75$ - Counter-rotating cylinder configurations

To account for the characteristic relaxation time of the suspension λ, Wiessenberg number Wi is defined as follows,

$$Wi^{(i,o)} = \frac{\lambda \cdot R_{i,o}}{|\Omega_{i,o} \cdot d_\beta|} \tag{2.4}$$

In addition, elasticity number El is used to quantify the importance between elastic and inertial effects as,

$$El = \frac{Wi}{Re} = \frac{\lambda\eta}{\rho d^2} \tag{2.5}$$

2.2 Morphological analysis

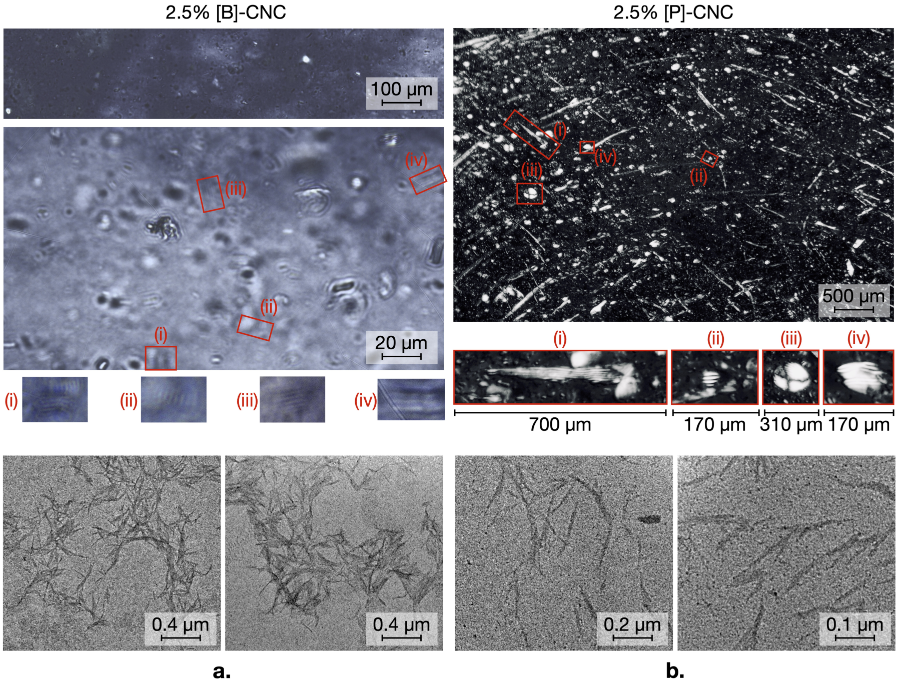

Figure 2.1: Polarized optical microscopy [POM] (Top) and Transmission electron microscopy [TEM] (bottom) images of a) 2.5 %[B]-CNC b) 2.5 %[P] CNC [Paper-I] [8]

The custom polarized light microscopy images in Fig 2.1 show the different structures, i.e. chiral nematic domains and agglomerates present in the CNC samples when prepared by different sample preparation methods at the microscopic length scale. Here, we can see that the amount of energy given to the sample in [B]-CNC is not enough to break those agglomerates present in the sample, whereas in [P] CNC, agglomerates were reduced, leading to the presence of more liquid crystalline tactoids (chiral nematic domains) in the sample[4]. Transmission electron microscopy (TEM) shows the differences in the number of aggregates and agglomerates present in the sample resulting from sample preparation methods at the nanoscale.

Small-angle X-ray scattering (SAXS)

SAXS experiments were performed mainly in CoSAXS and FORMAX beamlines at MAX IV Laboratory, Lund. Nanoscale orientation was obtained from the azimuthal integration of the scattering patterns using Hermans orientation parameter,

$$\langle P_2 \rangle_{SAXS} = \frac{\int_0^{\pi} \frac{1}{2}\left(3\cos^2\varphi - 1\right) I(\varphi)_q \sin\varphi d\varphi}{\int_0^{\pi} I(\varphi)_q \sin\varphi d\varphi} \tag{2.6}$$

where φ is the azimuthal angle of the scattering pattern, $I(\varphi)_q$ is the scattering intensity in the integrated q-range. Within the $[0, \pi]$ integration limits used in Eq. (2.6), $\langle P_2 \rangle_{SAXS} \in [-0.5, 1]$, where $\langle P_2 \rangle_{SAXS} = 0$ indicates randomly oriented nanoparticles, $\langle P_2 \rangle_{SAXS} = 1$ denotes fully oriented and $\langle P_2 \rangle_{SAXS} = -0.5$ with nanoparticles oriented in flow direction. We have used radial configuration of incident X-rays for Rheo-PLI-SAXS experiments whereas for TC-SAXS, tangential configuration was used. However for the paper-III, TC-SAXS experiments carried out at FORMAX with temporal resolution upto 100Hz to capture the nanoscopic dynamics inside the vortices [8], [22].

CHAPTER 3

Multiscale experiments

3.1 Hyphenated techniques

Hyphenated techniques uniquely characterize a material simultaneously at different lengths and time scales, which was not possible previously. Some of the methods presented here include Rheo-PLI-SAXS and TC-SAXS. This section summarizes the results obtained from multiscale experiments, revealing the nano-meso-macro scale propagation of orientation under shear and testing the influence of particle morphologies on Taylor vortices across nano-macro length scales with different sample preparation protocols.

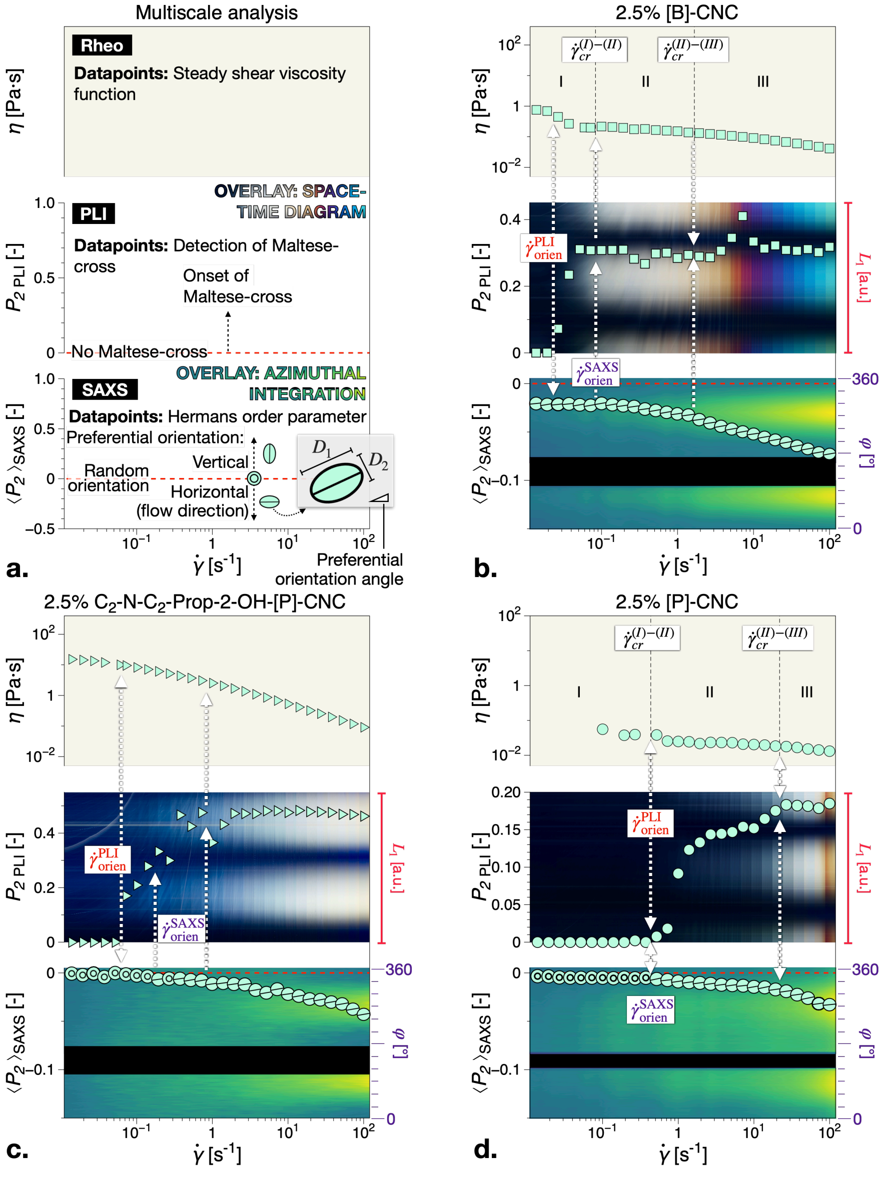

Figure 3.1: a) Overview of the multiscale analysis: Rheological data η vs $\dot{\gamma}$ [Top], Onset of the Maltese-cross pattern in the PLI Space-time diagram quantified based on Herman's orientation algorithm P_{2PLI} vs $\dot{\gamma}$ [Middle], Azimuthal integration of the scattering intensities from SAXS plotted as Hermans orientation parameter $< P_2 >_{SAXS}$ vs $\dot{\gamma}$; b) 2.5% [B] CNC, c) 2.5% [P]-CNC-OH-2-Prop-C_2-N-C_2, d) 2.5% [P] CNC [Paper-I] [8]

3.2 Rheo-PLI-SAXS [Paper-I]

For the first time, multiscale experiments have been performed on CNC suspensions ranging from magnetic stirred and bath sonicated sample [B], probe sonicated surface grafted CNC sample $[[P] - CNC - OH - 2 - Prop - C_2 - N - C_2]$ to probe sonicated commercial sulfated Celluforce CNCs with Na^+ as counter ion. An overview of the simultaneous rheological, polarized light imaging [PLI] and small-angle scattering experiments have been plotted in fig 3.1. Intriguing details of the orientation dynamics and propagation of the orientation happening at nano-micro length scales can be seen. The presence of agglomerates due to the addition of azetidinium salts onto the sulfate groups and non-probe sonicated Celluforce CNC sample exhibited different orientation responses to the applied shear rates. Experiments indicated the onset of mesoscale orientation, which could be identified by the Maltese-cross pattern, which precedes the nanoscale onset identified through SAXS. However, if the CNC sample includes primarily liquid crystalline domains with less number of agglomerates prepared through probe sonication for Celluforce CNCs, the nanoscale and mesoscale orientation onset occurs simultaneously. This provides insight into the orientation dynamics across different length scales.

3.3 Interplay between flow transitions and particle morphologies [Paper-II]

We have seen information on the multiscale assemblies responding to simple shear (parallel-plate flows) and its orientation onset in Paper-I. Now, we are exploring how the mesoscale assemblies stabilize/destabilize the flow or flow unwinds the same into primary nanoparticles in Taylor-Couette (TC) flow. We have taken two nanoparticles with different particle morphologies, including 1D CNCs (3wt%) with isotropic and chiral nematic domains and 2D GO (0.7 wt%) with mostly nematic domains. Here, the instabilities are seen through the custom polarized imaging TC setup where videos were recorded. Then the pixel from each video frame is extracted to form a space-time plot as shown in the top of fig 3.3. Later 2D FFT was performed to extract the spatial and temporal frequencies which varies with increase in rotation rates of the cylinder.

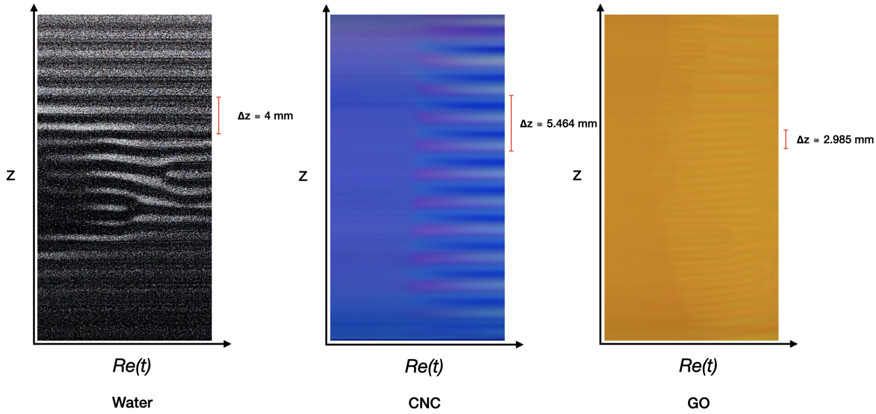

Figure 3.2: TVF onset for water, 1D CNC, 2D GO suspensions in $\beta = 0$ configuration [Paper-II]

.

With CNCs, shear-thinning modified the TVF onset identified through the stretching of vortices, leading to an increase in its axial size compared to water; $\Delta z = 2.732d$. GO sparks an interesting case showing an early sign of elasticity through its vortex size: $\Delta z = 1.49d$. Initially, the Taylor vortices emerge from both ends of the column and merge in the middle, as seen in CNCs at $Re_{TVF}^{\beta=0} = 223$. However, the GO's elasticity led to the emergence of Taylor vortices in the middle at $Re_{TVF}^{\beta=0} = 102$ and propagated to both ends. CNCs transition bifurcates from TVF into $WVF \rightarrow MWV \rightarrow CWV \rightarrow WTV$, corresponding to our setup's maximum Re and instability. GOs transitions were dominated mainly by shear thinning: $TVF \rightarrow WVF \rightarrow CS/W \rightarrow TWV \rightarrow TI$. Chaotic spiral waves (CS/W) are new kind of instability mode encountered in GO, where the vortices undergo chaotic behaviour in a spiral manner due to the interplay between elasticity and shear thinning disrupting the vortex size. This disruption is caused by their stretching and splitting which modify the transitions.

We have also tested the counter-rotating configurations [β = -0.5, -0.25, 0.75] and monitored their transition sequences. In the case of CNCs in $\beta = -0.25$, the transitions appear as LCF $\rightarrow$ TVF $\rightarrow$ WVF $\rightarrow$ MWV $\rightarrow$

CWV shown in Fig 3.3. For GO, apart from [$\beta = 0, -0.25$], all the other configurations stayed in laminar Couette flow till the maximum Re achieved in the setup. Spiral modes can be seen in $\beta = -0.25$ where the transitions appeared as LCF $\rightarrow$ PTVF $\rightarrow$ WVF $\rightarrow$ C/MWV $\rightarrow$ TI. Hybrid (CNCGO) exhibited a spiral mode at $\beta = 0$ rather than in the counter-rotating cylinder configuration. After LCF, the flow transitioned directly to spiral waves (S) $\rightarrow$ Wavy spirals (WS) $\rightarrow$ Chaotic wavy vortices (CWV). These modes have been identified in space-time plots and spectrograms. Interpenetrating spiral (IS) mode was present in both $\beta = -0.5$ & -0.25. For both GO and hybrid (CNCGO), LCF was present for the whole Re in $\beta = -0.75$ & -1. To account for the material's elasticity, the critical Weissenberg number($Wi_{cr}^{i,o}$) and the elasticity number (El) were plotted. All transitions of CNC, GO and CNCGO remained similar to those of a Newtonian fluid with modifications due to shearthinning, accompanied by their varied primary nanoparticle morphologies. Elastic effects were observed only in GO during the onset of TVF.

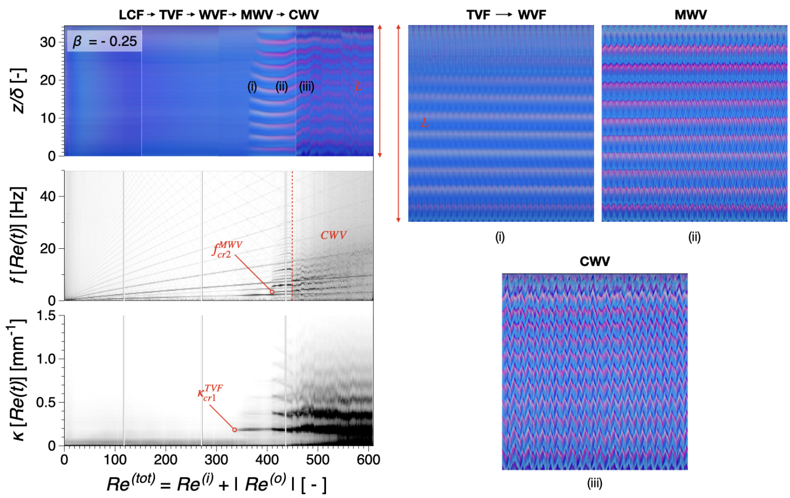

Figure 3.3: Transition sequences for the 1D suspension, $\beta = -0.25$ (counter-rotation). The left column contains the space time visualization (top), temporal spectrogram (middle) and spatial spectrogram (bottom). Instability modes are also highlighted on the right side. Note: $Re^{(i)} = Re^{(tot)}(1 - |\beta|)$, $Re^{(o)} = Re^{(tot)}|\beta|$ [Paper-II]

3.4 Nanoscale dynamics in transitional flow [Paper-III]

Narrowing the focus from macroscopic observations of vortices to the nanoscale is achieved by combining TC-PLI understanding with SAXS analysis and experiments. Vortex sizes, i.e. [Δz - resembles a pair of vortices], were calculated with the help of spatial wavenumbers obtained through the 2D-FFT analysis of PLI space-time plots 3.3 from TC flow. This gave us an insight into probing at the nanoscale using vortex size. We have found that CNCs and GOs exhibit intriguing dynamics with macroscopic frequencies that do not correlate with the nanoscopic frequencies of the former. In contrast, the latter shows a correlation between macroscopic and nanoscopic frequencies in a few instability modes. Moreover, GO had a destabilizing effect on the instabilities, while CNCs had a stabilizing effect.

CHAPTER 4

New Rheo-non linear optics setup

Here, the theory behind some of the nonlinear optical techniques, such as second-harmonic generation (SHG) and the preliminary experimental design comprising different components, were discussed.

4.1 Theoretical aspects

In conventional (linear) optics, the polarization response $\tilde{P}$ (t) (the dipole moment per unit volume) of a material system is linearly dependant on the applied electric field $\tilde{E}(t)$,

$$\tilde{P}(t) = \epsilon_0 \chi^{(1)} \tilde{E}(t) \tag{4.1}$$

- $\chi^{(1)}$ is the linear susceptibility,
- ϵ_0 is the vacuum permittivity,
- $\sim$ denotes the quantities which vary rapidly in time.

When an intense high power laser is used, the generated polarization response from the material will be nonlinear which can be expanded in the Taylor series expansion as

$$\tilde{P}(t) = \epsilon_0 \left[\chi^{(1)}\tilde{E}(t) + \chi^{(2)}\tilde{E}^2(t) + \chi^{(3)}\tilde{E}^3(t) + \cdots\right] \tag{4.2}$$

$$\equiv \tilde{P}^{(1)}(t) + \tilde{P}^{(2)}(t) + \tilde{P}^{(3)}(t) + \cdots \tag{4.3}$$

where,

- $\tilde{P}^{(2)}(t) = \epsilon_0\chi^{(2)}\tilde{E}^2(t)$ is the second-order non-linear polarization such as SHG,
- $\tilde{P}^{(3)}(t) = \epsilon_0\chi^{(3)}\tilde{E}^3(t)$ is the third-order nonlinear polarization such as third harmonic generation (THG),
- $\chi^{(2)}$, $\chi^{(3)}$ are second and third-order nonlinear optical susceptibilities.

For the SHG process, when an electric field with an angular frequency ω is incident on a non-centrosymmetric medium with $\chi^{(2)}$ as nonzero, the total electric field can be expressed in complex notation as

$$\tilde{E}(t) = Ee^{-i\omega t} + E^*e^{i\omega t} \tag{4.4}$$

- E is complex amplitude of the electric field,
- E^* is its complex conjugate.

The propagation of the electric field in a nonlinear dielectric medium is governed by the inhomogeneous wave equation derived from Maxwell's equations. In the presence of a second-order nonlinear polarization, the equation takes the form:

$$\nabla^2\tilde{E} - \frac{n^2}{c^2}\frac{\partial^2\tilde{E}}{\partial t^2} = \frac{1}{\epsilon_0 c^2}\frac{\partial^2\tilde{P}^{\mathrm{NL}}}{\partial t^2} \tag{4.5}$$

Here:

- n is the linear refractive index,
- c is the speed of light in vacuum,

- $\tilde{P}^{\mathrm{NL}}$ is the second-order nonlinear polarization (source term)
- The right hand side of the equation describes the radiation generated by the accelerated charges associated with nonlinear polarization [23].

4.2 Preliminary design of nonlinear optical microscopy/spectroscopy

The experimental setup for Rheo-SHG microscopy/spectroscopy involves a polarizer [P], analyzer [A], quarter wave plate [QWP], beamsplitter [BS], mirrors [M], objective lens [L], tube lens [TL], and detector [D] and the parallel plate [PP] measuring geometry of the rheometer as shown in Fig 4.1.

Laser

We need high-peak-powered lasers to generate a nonlinear response from a material. Here, Thorlabs TIBERIUS Ti-Sapphire femtosecond laser with a tunable wavelength from 720 - 1060 nm and an average output power of 2 W @ 800 nm is used in the setup. The laser is mode-locked at a pulse width of 140 fs and a 77 MHz repetition rate. The laser has a beam diameter of 1.5 mm and a peak pulse power of 213 kW.

Polarizer

Thorlabs GL10—Mounted Glan-Laser Polarizer, Ø10 mm CA, Uncoated are used as polarizers and analyzers in the setup. The uncoated version allows us to polarize the whole range of the excitation laser wavelength from 720-1060 nm and also the emitted signals from the sample. These polarizers are mounted on a Thorlabs high-precision rotation mount to rotate the polarizing angle of the excitation and emitted signals.

Quarter waveplate

Superachromatic Quarter-Wave Plate with a transmission wavelength from 325 - 1100 nm by Thorlabs [SAQWP05M-700] is used to delay the slow axis of the two electric field components (E_x & E_y)of the linearly polarized light from the polarizer. This, in turn, introduces the phase shift of 45^0 between the two orthogonal components E_x & E_y, converting the linear to a circularly polarized light.

Mirrors

Right-angle prism mirrors from Thorlabs with a protected silver coating reflect wavelengths from 450 nm to 20 µm. These mirrors steer the beam by reflecting it in the specified direction.

Beam splitter

Thorlabs [DMSP680B] Shortpass Dichroic Mirror is used to split and reflect the beam using a beamsplitter. This dichroic mirror has a transmission band of 400 - 660 nm and a reflection Band from 705 - 1080 nm with a 680 nm Cutoff. So that the excitation input from the laser and the emitted signal from the sample can be directed onto the same mirror, thereby minimizing the need to use multiple mirrors and filters. Based on the forward or backward detection mode, the beamsplitter's entry and exit points can be changed accordingly to accommodate the signals.

Lens

Two dry objective lenses from Thorlabs [TL10X-2P] are used to focus the excitation beam onto the sample and collect the emitted signals from the sample. This lens is suitable for the setup with multiphoton detection capabilities ranging from 400-1300 nm wavelength with a working distance (WD) of 7.77 mm and a numerical aperture (NA) of 0.5. It has a correction collar to accommodate the spherical aberrations caused by thick samples or aqueous solutions. A 200 mm focal length tube lens [TTL200MP] converts the rays from the objective to form an image or focus on the detector at a distance.

Detector

The setup consists of two types of detectors: a photomultiplier tube (PMT) and an intensified CMOS camera (istar sCMOS).

PMT

A Gallium Arsenide Phosphide photomultiplier tube (PMT) from Thorlabs [PMT2101/M] is used for the point source detection of emitted signals from the sample. It has a detection range of 300-720 nm, high sensitivity at 550 nm, and an active area of 5 mm. It is used for the detection of low-sensitive SHG or TPEF signals, photon counting measurements, and imaging when a scanner is used to rasterize the sample.

Camera

The istar sCMOS intensified camera from Oxford instruments is used to image and detect the emitted signals at ultrafast timescales. A phosphor screen is used in front of the CMOS sensor as an intensifier to block unwanted photons that hit the sensor, allowing us to achieve a temporal resolution up to 2 ns. The camera features a sensor matrix of 2560 x 2160 pixels (WXH), with a pixel size of 6.5μm and a wavelength range of 180 - 850 nm.

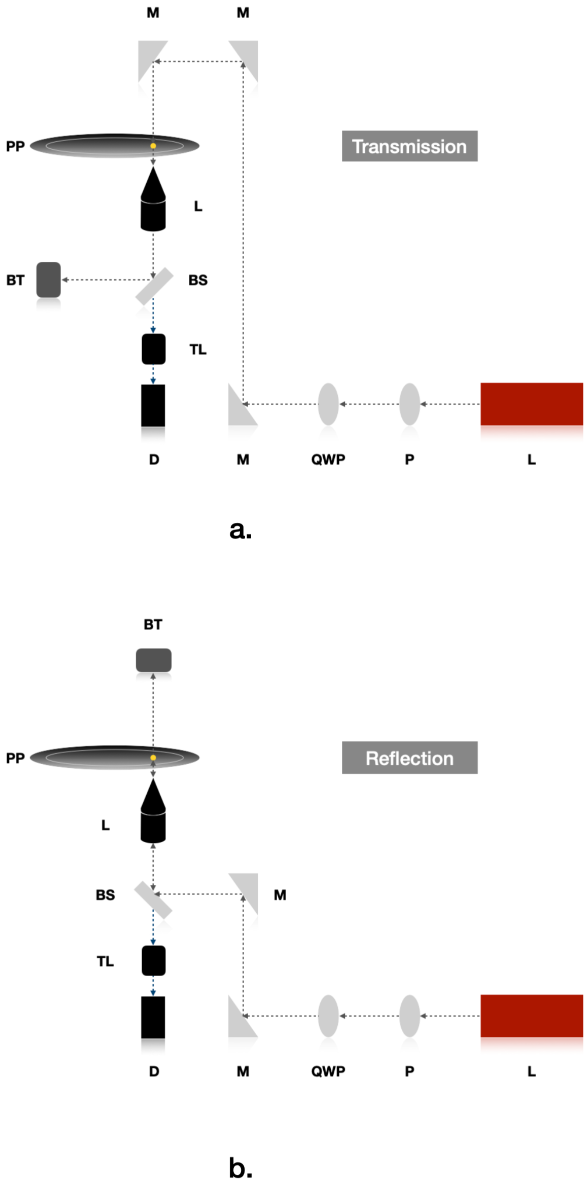

Figure 4.1: Schematic of the experimental setup: a) Transmission mode , b) Reflection mode

CHAPTER 5

Conclusion and future work

The dynamics of hierarchical nanostructured fluids across multiple length and time scales have been studied here. In Paper I, we have explored the first multiscale experiment on different CNC suspensions where the orientation onset precedes or succeeds between shear rates altered by surface modification and sample preparation protocol. In Paper II, CNC and GO impact the flow transitions in TC flow, showing signs of primary instability; TVF modified by shear thinning for the former, with the latter being attributed to elasticity despite all transitions showing similarities to a Newtonian fluid. In Paper III, we delved deeper into the vortex dynamics at the nanoscale, building on our understanding from Paper II, which revealed some instability mode frequencies correlate with both macro and nano scales for GO, while CNC exhibited contrasting dynamics. In addition, a new Rheo-nonlinear optics setup is being developed to understand mesoscale dynamics, thereby minimizing the unknowns across length and time scales.

5.1 Future work

Based on the experiments and developments done, the work mentioned in this thesis will be further explored and extended as follows,

- More accurate quantitative information can be obtained with a high-speed polarization camera, increasing the temporal resolution and orientation monitored through the stress-induced retardation values, which are currently being developed.
- Expanding the multiscale analysis to different materials like 2D nanoparticles in simple shear.
- Mainly, Rheo-NLO will be developed to understand the mesoscale evolution of hierarchical systems where SHG and TPEF plan to be explored as nonlinear optical microscopy techniques.
- Moreover, the above ultrafast time scales up to nanoseconds will be achieved for both quantitative and qualitative means obtained from the nonlinear polarization response of the hierarchical systems.
- Nonlinear rheology will be explored in multiscale analysis.

References

[1] C. Chen, Y. Kuang, S. Zhu, *et al.*, "Structure–property–function relationships of natural and engineered wood," *Nature Reviews Materials*, vol. 5, no. 9, pp. 642–666, 2020.

[2] R. M. Parker, G. Guidetti, C. A. Williams, *et al.*, "The self-assembly of cellulose nanocrystals: Hierarchical design of visual appearance," *Advanced Materials*, vol. 30, no. 19, p. 1 704 477, 2018.

[3] Z. Xu and C. Gao, "Aqueous liquid crystals of graphene oxide," *ACS nano*, vol. 5, no. 4, pp. 2908–2915, 2011.

[4] T. G. Parton, R. M. Parker, G. T. Van De Kerkhof, *et al.*, "Chiral self-assembly of cellulose nanocrystals is driven by crystallite bundles," *Nature Communications*, vol. 13, no. 1, p. 2657, 2022.

[5] H. A. Barnes, J. F. Hutton, and K. Walters, *An introduction to rheology*. Elsevier, 1989, vol. 3.

[6] R. Kádár, S. Spirk, and T. Nypelo, "Cellulose nanocrystal liquid crystal phases: Progress and challenges in characterization using rheology coupled to optics, scattering, and spectroscopy," *ACS nano*, vol. 15, no. 5, pp. 7931–7945, 2021.

[7] R. Kádár, A. Terry, K. Nygård, *et al.*, "Challenges in nano-structured fluid flows for assembly into hierarchical biomaterials," in *AIP Conference Proceedings*, AIP Publishing, vol. 2997, 2023.

[8] R. Ghanbari, A. Terry, S. Wojno, *et al.*, "Propagation of orientation across lengthscales in sheared self-assembling hierarchical suspensions via rheo-pli-saxs," *Advanced Science*, vol. 12, no. 7, p. 2 410 920, 2025.

[9] R. J. Donnelly, "Taylor–couette flow: The early days," *Phys. Today*, vol. 44, no. 11, pp. 32–39, 1991.

[10] P. G. Drazin and W. H. Reid, *Hydrodynamic stability*. Cambridge university press, 2004.

[11] M. Fardin, C. Perge, and N. Taberlet, ""the hydrogen atom of fluid dynamics"–introduction to the taylor–couette flow for soft matter scientists," *Soft Matter*, vol. 10, no. 20, pp. 3523–3535, 2014.

[12] C. D. Andereck, S. Liu, and H. L. Swinney, "Flow regimes in a circular couette system with independently rotating cylinders," *Journal of fluid mechanics*, vol. 164, pp. 155–183, 1986.

[13] C. S. Dutcher and S. J. Muller, "Spatio-temporal mode dynamics and higher order transitions in high aspect ratio newtonian taylor–couette flows," *Journal of fluid mechanics*, vol. 641, pp. 85–113, 2009.

[14] R. Kádár and C. Balan, "Transient dynamics of the wavy regime in taylor–couette geometry," *European Journal of Mechanics-B/Fluids*, vol. 31, pp. 158–167, 2012.

[15] C. S. Dutcher and S. J. Muller, "Effects of weak elasticity on the stability of high reynolds number co-and counter-rotating taylor-couette flows," *Journal of Rheology*, vol. 55, no. 6, pp. 1271–1295, 2011.

[16] C. S. Dutcher and S. J. Muller, "Effects of moderate elasticity on the stability of co-and counter-rotating taylor–couette flows," *Journal of Rheology*, vol. 57, no. 3, pp. 791–812, 2013.

[17] R. Ghanbari, S. Pashazadeh, K. Sekar, *et al.*, "Painting taylor vortices with cellulose nanocrystals: Suspension flow supercritical spectral dynamics," *Physics of Fluids*, vol. 36, no. 4, 2024.

[18] X. Chen, O. Nadiarynkh, S. Plotnikov, and P. J. Campagnola, "Second harmonic generation microscopy for quantitative analysis of collagen fibrillar structure," *Nature protocols*, vol. 7, no. 4, pp. 654–669, 2012.

[19] T. Legat, V. Grachev, D. Kabus, *et al.*, "Imaging with a twist: Three-dimensional insights of the chiral nematic phase of cellulose nanocrystals via shg microscopy," *Science Advances*, vol. 10, no. 44, eadp2384, 2024.

[20] J. K. Wychowaniec, M. Iliut, B. Borek, *et al.*, "Elastic flow instabilities and macroscopic textures in graphene oxide lyotropic liquid crystals," *npj 2D Materials and Applications*, vol. 5, no. 1, p. 11, 2021.

[21] P. Munier, S. E. Hadi, M. Segad, and L. Bergström, "Rheo-saxs study of shear-induced orientation and relaxation of cellulose nanocrystal and montmorillonite nanoplatelet dispersions," *Soft Matter*, vol. 18, no. 2, pp. 390–396, 2022.

[22] K. Nygård, S. McDonald, J. González, *et al.*, "Formax–a beamline for multiscale and multimodal structural characterization of hierarchical materials," *Synchrotron Radiation*, vol. 31, no. 2, pp. 363–377, 2024.

[23] R. W. Boyd, A. L. Gaeta, and E. Giese, "Nonlinear optics," in *Springer Handbook of Atomic, Molecular, and Optical Physics*, Springer, 2008, pp. 1097–1110.